Preprints (www.preprints.org) | NOT PEER-REVIEWED | Posted: 13 October 2020 doi:10.20944/preprints202010.0260.v1

Article

High-frequency heat treatment of AISI 1045 specimens and current calculations of the induction heating coil using metal phase transformation simulations

Jinkyu Choi [1] and Seoksoon Lee [1,*]

[1] Department of Mechanical Engineering and Engineering Research Institute, Gyeongsang National University, 501, Jinju-daero, Jinju-si, Gyeongsangnam-do 52828, Korea, jinkyu87@gnu.ac.kr

* Correspondence: leess@gnu.ac.kr; Tel.: +82-55-772-1622

Abstract: Based on electromagnetic heat transfer and metal phase transformation co-simulations, we modeled an AISI 1045 specimen under high-frequency heat treatment. Hardening zone predictions were confirmed through cooling and metal phase transformation simulations after obtaining the results from electromagnetic heat transfer simulations. The cooling process was modeled by applying the cooling coefficient of the cooling water in the same way as the actual heat-treatment process. To obtain the current flowing through the coil during high-frequency induction heating, the voltage was measured and applied using the resistance–inductance–capacitance circuit calculation method. Experimental and simulated results of the heating temperature and curing depth of an AISI 1045 specimen with a carbon content of 0.45% were compared; the comparison indicated good agreement between the two. Using the simulation results, we established a method for obtaining the current flowing through the induction coil for predicting the extent and depth of the hardening zone during high-frequency induction heat treatment.

Keywords: AISI 1045; Co-simulation; High-Frequency Induction Heat Treatment; Metal Phase Transformation; RLC Circuit

1. Introduction

The biggest issues in heat treatment applications often involve improving the energy efficiency, improving the product quality, and minimizing environmental pollutants and CO2 emissions during the heat treatment process. High-frequency induction hardening is economical and environmentally friendly, as heat energy is created using electricity instead of burning fossil fuels. Due to these advantages, it is widely used as a local hardening heat treatment technology.

In high-frequency induction hardening, quality is determined by various parameters, such as the input power, heating and cooling times, the shape of the heating coil, and the shape and material of the object to be heated/hardened. At present, these variables are determined by the experience of skilled workers who produce the product through trial and error. Since the 1970s, various methods have been applied to better understand these parameters and reduce unnecessary losses during the induction hardening process. One such method is finite element analysis. Han et al. [1] simulated heat treatment using middle-frequency induction heating of welded pipes. Li et al. [2] optimized ball screw processing variables based on induction hardening simulations. Lee et al. [3] compared the results from temperature measurement experiments and finite element analyses under high-frequency induction heating of AISI 4140 round bars. Oh et al. [4] calculated the induction heating coil temperature distribution from design parameters, such as the radius and thickness. Ji et al. [5] used finite element analyses to design a rolling process for gear manufacturing using high-frequency induction heating. Tak et al. [6] conducted a study to improve formability by heating an object by induction heating. Choi et al. [7,8] conducted finite element analyses of induction hardening of a

© 2020 by the author(s). Distributed under a Creative Commons CC BY license.

Preprints (www.preprints.org) | NOT PEER-REVIEWED | Posted: 13 October 2020 doi:10.20944/preprints202010.0260.v1

sprocket; the input power in the induction hardening heat treatment process of an AISI 1045 round bar was considered, and the results showed the hardening region obtained by heating and cooling analyses, which was compared to that obtained experimentally. Numerous studies have examined the phase changes that occur with temperature during induction heating. Tong et al. [9] conducted high-frequency induction hardening experiments and simulations of JIS-SCM440 using co-simulation of the electromagnetic heat transfer process and metal phase transformation. However, studies of high-frequency induction heating and hardening utilizing finite element analysis have not considered the input power of the process variables.

In this study, after measuring the input power in the induction hardening treatment of an AISI 1045 specimen, the current flowing through the induction heating coil was calculated and applied to the simulation. The accuracy of the simulation of high-frequency induction hardening was improved by comparing and analyzing the hardening depth obtained experimentally with that obtained from simulations based on the current in the induction heating coil.

2. High-frequency induction hardening process of the AISI 1045 specimen

2.1. High-frequency induction hardening procedure

A high frequency induction hardening experiment was performed using a specimen of AISI 1045 steel with a diameter of 10 mm and a length of 100 mm and a 6 kW high frequency induction heating device. For the induction hardening heat treatment of the AISI 1045 specimen, the working conditions are applied as shown in Fig. 1. The frequency is 242 kHz, the input voltage is DC 207 V, the input current is DC 23 A, and it is cooled for 6 seconds after heating for 2 seconds with a total input power of 4.8 kW. High-frequency heat treatment is a process of rapidly cooling carbon steel below Ms (Martensitic transformation start temperature) after heating above A1 transformation point temperature. The A1 transformation point temperature of the parking gear with a carbon content of 0.45% is 727 ℃[10] and the heating temperature of the specimen is measured using a thermal imaging camera Fluke Ti450 pro same as Fig. 2.

2.2. High-frequency induction hardening results

A total of six measurements were made as shown in Fig. 3, and the average heating temperature was 798.5 ℃. It was confirmed that it was heated above the A1 transformation point temperature. To measure the hardening depth of a specimen subjected to high-frequency heat treatment, After the specimen was made as shown in Fig. 4, the hardening depth was measured using a micro-Vickers hardness tester after etching using a nital corrosion solution of 3%. As a result of measuring the hardening depth based on Hv 450 as a reference[11], the hardening depth in the center was 0.8 mm.

< Working conditions >

- Voltage : 207 V
- Ampere : 23 A
- Power : 4.8 kW
- Frequency : 242 kHz
- Heating time : 2 sec
- Cooling time : 6 sec

Figure 1. High-frequency induction hardening working conditions for the AISI 1045 specimen.

Preprints (www.preprints.org) | NOT PEER-REVIEWED | Posted: 13 October 2020 doi:10.20944/preprints202010.0260.v1

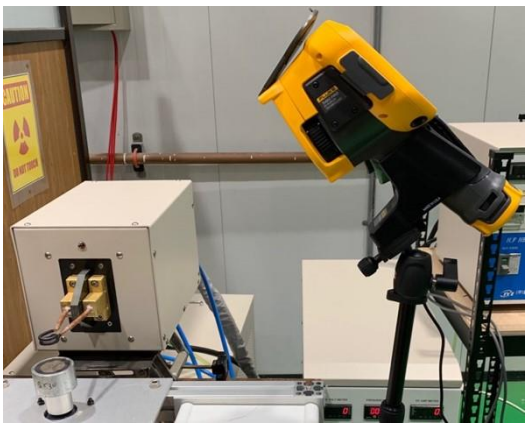

Figure 2. Measurement temperature setup for the AISI 1045 specimen during induction heating.

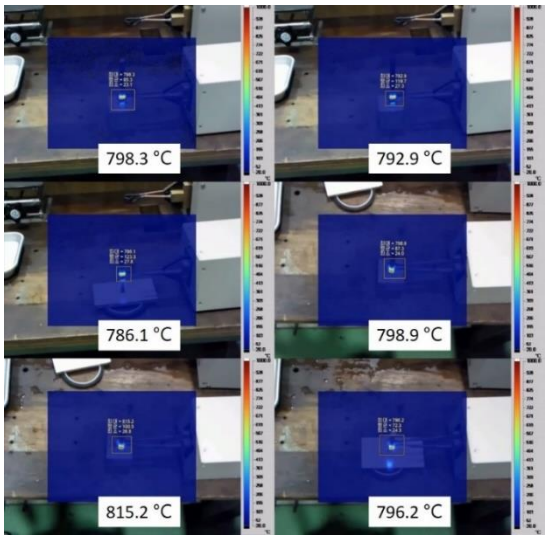

Figure 3. Measurement temperature results of AISI 1045 specimens during induction heating.

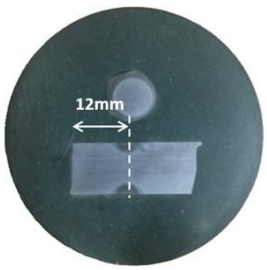

◇ Micro Vickers hardness test conditions : load 300g / 12sec

Category		Surface section				Near surface section														Deep section			Center
2.0 sec	Depth[mm]	0.05	0.10	0.15	0.20	0.30	0.40	0.50	0.60	0.70	0.80	0.90	1.00	1.10	1.20	1.30	1.40	1.50	1.60	2.00	3.00	4.00	5.00
	Vickers Hardness [Hv]	520	573	580	600	584	590	485	498	492	500	431	409	363	367	316	334	328	269	251	258	260	265
	Rockwell Hardness [HrC]	50.5	53.8	54.2	55.3	54.4	54.7	48.1	49	48.6	49.1	43.8	41.8	37	37.5	31.8	33.8	33.2	25.7	22.6	23.8	24	25

When the carbon content of the steel is 0.43-0.53%, the effective hardness is up to **Hv 450**

Reference : KS D 0027 (Material part of Korean Industrial Standards)

Figure 4. Measurement hardening depth results of the AISI 1045 specimen.

3. Calculation of induction coil current

To simulate the high-frequency induction hardening process of the AISI 1045 specimen, the current value flowing through the coil during heating must be known. Given that a high current of high frequency cannot be measured directly, it is calculated by applying a voltage to a resistance–inductance–capacitance (RLC) circuit. Figure 5 shows a configuration diagram of the high-frequency

Preprints (www.preprints.org) | NOT PEER-REVIEWED | Posted: 13 October 2020 doi:10.20944/preprints202010.0260.v1

induction heating system. The alternating current (AC) is converted into DC current via a converter. Then the DC power is converted into AC electricity of the desired frequency to perform induction heating. To calculate the current flowing through the induction coil, an oscilloscope was used to measure the voltage and frequency in the transformer and coil of the CT-BOX of the high-frequency induction heating system; here, the CT-BOX effectively acts as the RLC circuit. The input power of the high-frequency heat treatment system is listed in Table 1. The voltage was 207 V/DC, the current was 23 A/DC, the frequency was 242 kHz, and the total power was 4.8 kW. Figure 6 shows the measurement sections of the CT-BOX; the voltage and frequency of measurement sections 1 and 2 were 241.7 kHz and AC 130 V and 242 kHz and AC 194 V, respectively (Table 2).

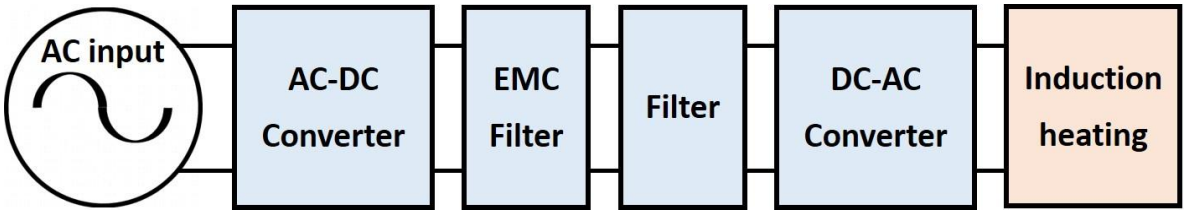

Figure 5. Configuration of high-frequency induction heating system.

Table 1. Input power of the induction heating device.

	DC Voltage [V]	DC Current [A]	Frequency [kHz]	Input power [kW]
Value	207	23	242	4.8

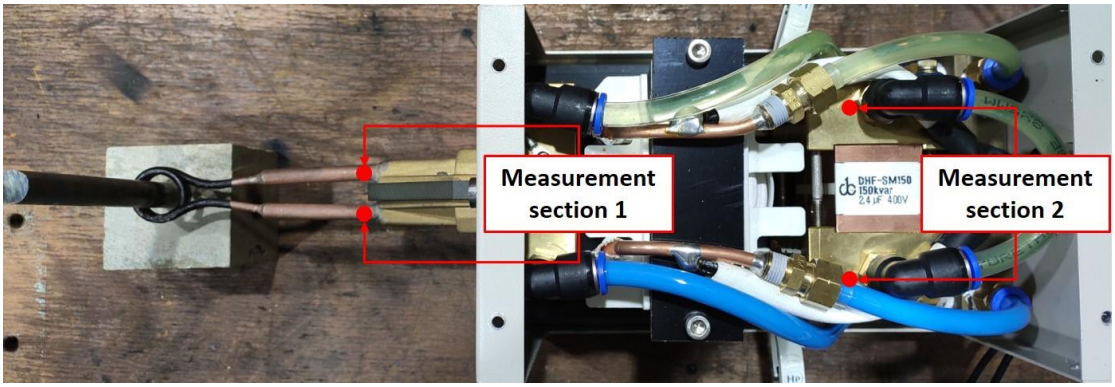

Figure 6. Position of the measurement sections in CT-BOX.

Table 2. Measurement results for the alternating current voltage and frequency in measurement sections 1 and 2.

	AC Voltage [V]	AC Current [A]
Measurement section 1	130	241.7
Measurement section 2	194	242

Preprints (www.preprints.org) | NOT PEER-REVIEWED | Posted: 13 October 2020 doi:10.20944/preprints202010.0260.v1

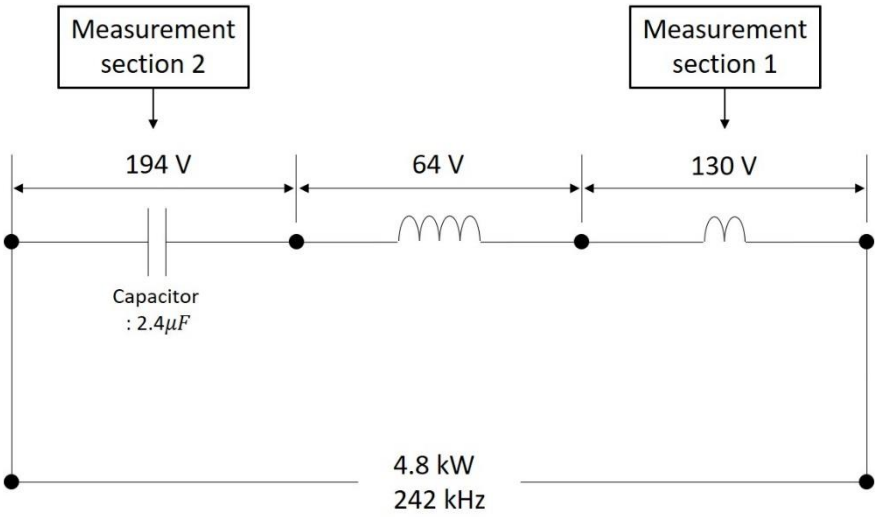

Figure 7. Voltage, frequency, and the representative resistance–inductance–capacitance (RLC) circuit of the CT-BOX for measurement sections 1 and 2.

To calculate the current flowing through the induction heating coil, the CT-BOX of the high-frequency induction heating system was displayed represented by an RLC circuit, as shown in Fig. 7. The input voltage, power, frequency, and the 2.4 $\boldsymbol{\mu F}$ capacitor value of the CT-BOX are displayed in the figure.

To calculate the current flowing through the induction heating coil, the CT-BOX of the high-frequency induction heating system was represented by an RLC circuit, as shown in Fig. 7. The input voltage, power, frequency, and the 2.4 $\boldsymbol{\mu F}$ capacitor value of the CT-BOX are displayed in the figure. Capacitive reactance $\boldsymbol{X_C}$ and inductance reactance $\boldsymbol{X_L}$ are required to calculate the frequency of the CT-BOX of the high-frequency induction heating device, as represented by a series RLC circuit [12]. The value of $\boldsymbol{X_C}$ is given by Eq. (1); a value of 0.274 Ω was confirmed. In the series RLC circuit, $\boldsymbol{X_C}$ and $\boldsymbol{X_L}$ are the same; thus, the inductance L can be calculated using Eq. (2) to obtain XL. The resonant frequency, Eq. (3), was calculated using inductance $\boldsymbol{L}$ and capacitor $\boldsymbol{C}$. The calculated resonant frequency coincided with the measured frequency. A current value of 708 A was obtained using Eq. (4) and (5) based on the capacitor and inductance values given.

$$X_C = \frac{1}{2\pi fC} = \frac{1}{2\pi \times 242000 \times 2.4 \times 10^{-6}} = 0.274\ \Omega \quad (1)$$

$$X_L = 2\pi fL = 0.274\ \Omega \rightarrow L = \frac{0.274}{2\pi \times 242000} = 1.8 \times 10^{-7}\ H \quad (2)$$

$$f_r = \frac{1}{2\pi\sqrt{LC}} = \frac{1}{2\pi\sqrt{1.8 \times 10^{-7} \times 2.4 \times 10^{-6}}} = 242146\ Hz = 242\ kHz \quad (3)$$

$$I_C = \frac{V_{max}}{X_C} = V \cdot 2\pi fC = 194 \times 2\pi \times 242146 \times 2.4 \times 10^{-6} = 708\ A \quad (4)$$

$$I_L = \frac{V_{max}}{X_L} = \frac{V_{max}}{2\pi fL} = \frac{194}{2\pi \times 242146 \times 1.8 \times 10^{-7}} = 708\ A \quad (5)$$

4. Simulations of the high-frequency induction hardening process

To verify the calculated current of the induction heating coil, as shown in Fig. 8, the specimen and coil were modeled in three dimensions. The simulation processes for electromagnetic heat transfer and metal phase transformation coupling are shown in Fig. 9. Eddy currents generated by

Preprints (www.preprints.org) | NOT PEER-REVIEWED | Posted: 13 October 2020 doi:10.20944/preprints202010.0260.v1

magnetic fields are generated during induction heating. Joule heat is created due to the eddy currents, and the temperature of the specimen rises. When the temperature of the specimen is heated above the A1 transformation point, a phase change occurs in the metal, resulting in changes to the properties of the metal. During the cooling process, when the temperature of the specimen is rapidly cooled from the A1 transformation point to the MS temperature, the metal phase and the material properties change once again. Figure 10 shows the curve of the thermal and electromagnetic properties of AISI 1045 steel, including the heat conductivity, relative permeability, electrical conductivity, and specific heat as a function of the temperature [13]. The Curie temperature of AISI 1045 steel is 727 ℃. In Fig. 8(c) and (d), the ferromagnetic properties were lost when the temperature exceeded the Curie temperature during induction heating. The effects of change in the relative permeability due to phase change were negligible.

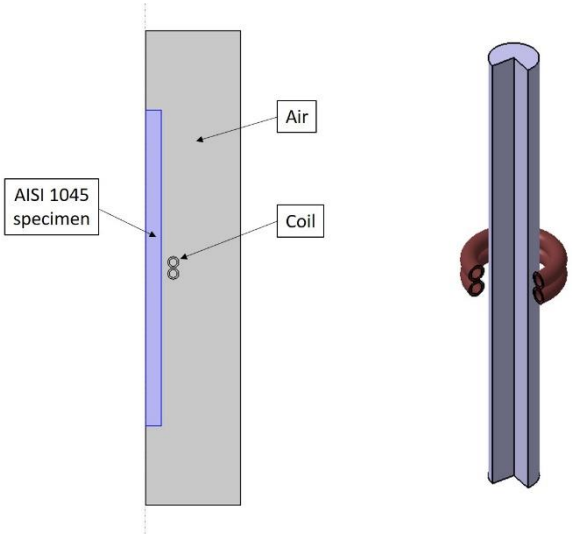

Figure 8. 3D model for induction hardening simulation.

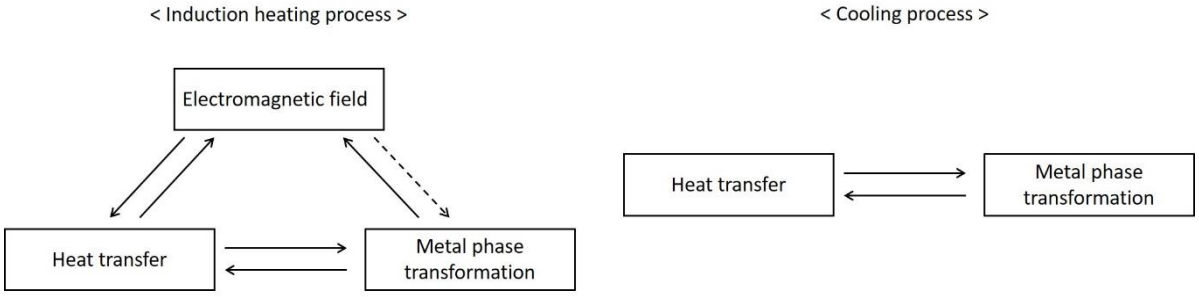

Figure 9. Induction hardening simulation process. The dashed line does not couple during the simulation.

The phase change of AISI 1045 depends on the temperature during high-frequency induction heating. The phase transformation of ferrite to austenite was modeled using the Leblond–Devaux phase transformation model, due to its diffusion characteristics. The temperature-dependent function that describes the phase change is shown in Table 3. The time rate of change in the fraction of austenite formed at the expense of ferrite is given by Eq. (6) [14]. Unlike the diffusion phase transformation of austinite, the phase transformation of martensite is distributed, and the proportion of formed martensite is proportional to overcooling to the MS temperature or lower, as given by the Koistinen–Marburger model. The rate of change in martensite is described by Eq. (7) and is listed in Table 4 [15].

$$\dot{\xi}^d = K(T)\xi^S - L(T)\xi^d \quad (6)$$

$$\dot{\xi}^d = -\xi^S \beta \dot{T} \quad (7)$$

Preprints (www.preprints.org) | NOT PEER-REVIEWED | Posted: 13 October 2020 doi:10.20944/preprints202010.0260.v1

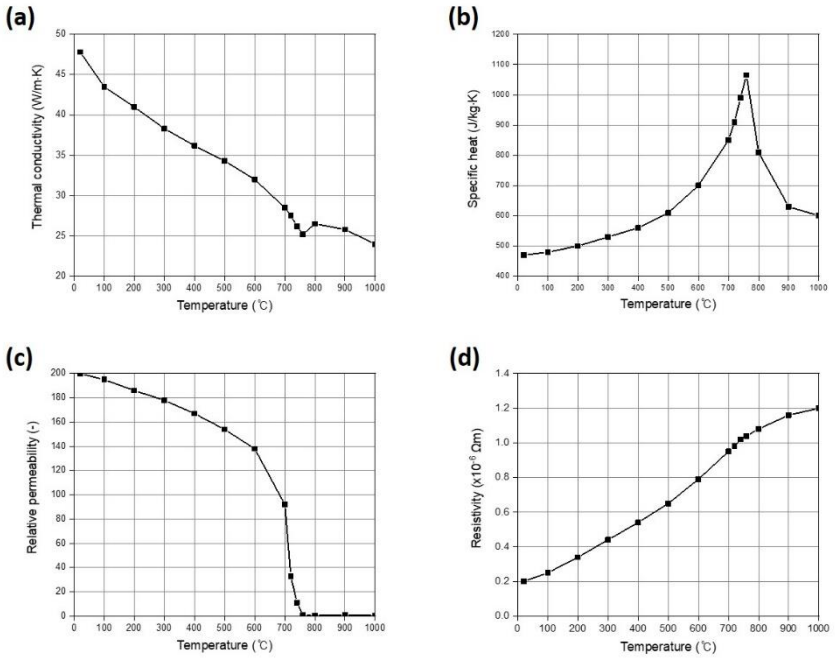

Figure 10. Thermal and electromagnetic properties with temperature of AISI 1045 steel. (a) Thermal conductivities, (b) specific heat, (c) relative permeability, (d) resistivity.

Table 3. Ferrite to austenite temperature-dependent functions.

Temperature [℃]	K [l/s]	L [l/s]
600	0.0001	0
620	0.0018	0.0002
800	0	0.002

Table 4. Austenite to martensite parameters.

Parameter	Value
M_S	370 [℃]
β	0.011 [1/K]

When the AISI 1045 specimen was heated for 2 s with a high-frequency alternating current of 708 A at 242 kHz, the maximum temperature reached during heating was 813 ℃, as shown in Fig. 11 (a). Cooling for 6 s after heating was simulated with reference to the heat transfer coefficient of water spray by Edelbauer et al. [16]. The maximum temperature was 201 ℃ (Fig. 11b). After about 2 s of high-frequency induction heating, the phase changed to austenite beyond the temperature of the A1 transformation point, and then the specimen was heated to a maximum temperature of 813 ℃. During cooling, it can be predicted that the phase will change from austenite to martensite by being rapidly cooled to the MS temperature or less within 1.5 s. The high-frequency induction heating and

Preprints (www.preprints.org) | NOT PEER-REVIEWED | Posted: 13 October 2020 doi:10.20944/preprints202010.0260.v1

cooling simulation results of the AISI 1045 specimen indicated that the phase change was achieved. The results of phase change simulations during high-frequency heat treatment are shown in Fig. 12. Figure 12(a) shows the phase conversion status of the AISI 1045 specimen when induction heating was performed for 2 s. The phase transition was one from ferrite to austenite. If the austenite cools rapidly, the martensite changes phase. Figure 12(b) shows the distribution of martensite when cooled for 4 s after induction heating. Through this, phase conversion during high-frequency heat treatment simulations was confirmed. To predict the hardening depth of the AISI 1045 specimen, the predicted hardening depth was measured on the martensite distribution plot, as shown in Fig. 13, in which a hardening depth of 0.8 mm was projected.

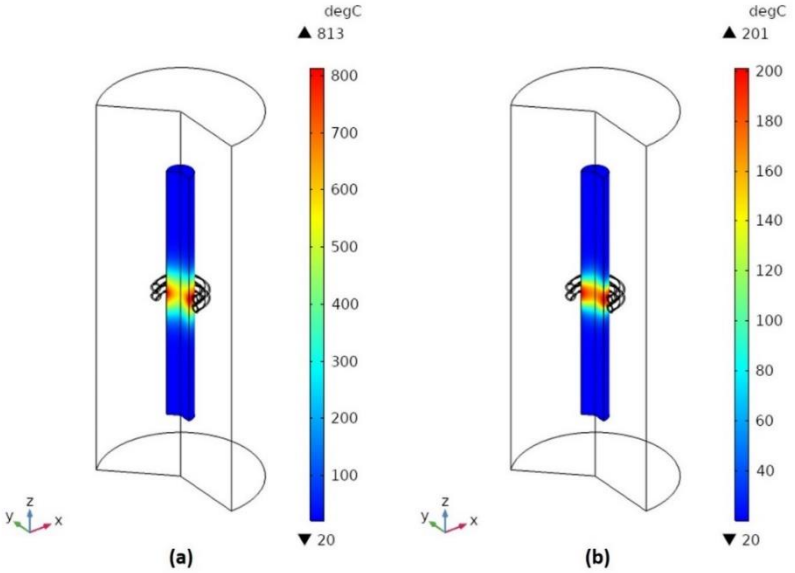

Figure 11. Induction heating simulation results: (a) 2 s after heating and (b) 4 s after cooling.

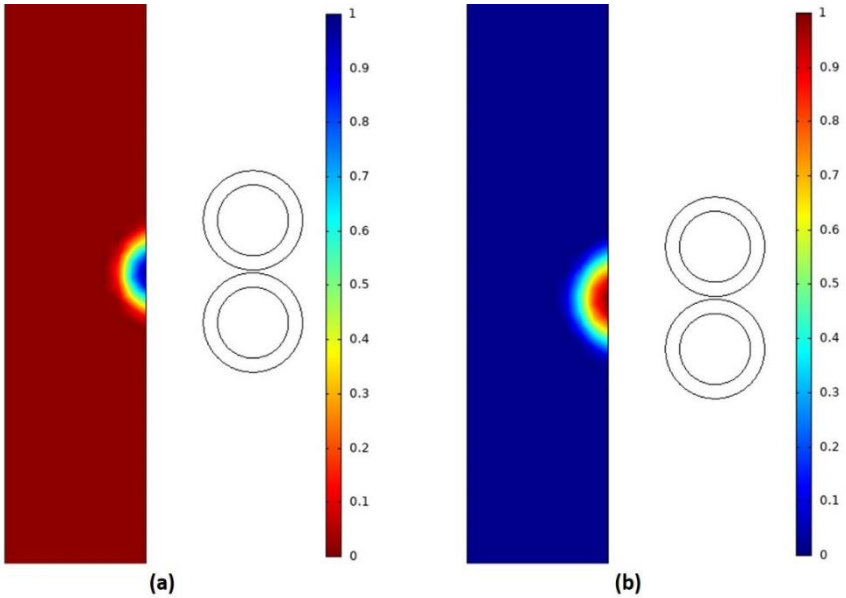

Figure 12. Phase change simulation results of AISI 1045 specimens: (a) austenite and (b) martensite.

Preprints (www.preprints.org) | NOT PEER-REVIEWED | Posted: 13 October 2020 doi:10.20944/preprints202010.0260.v1

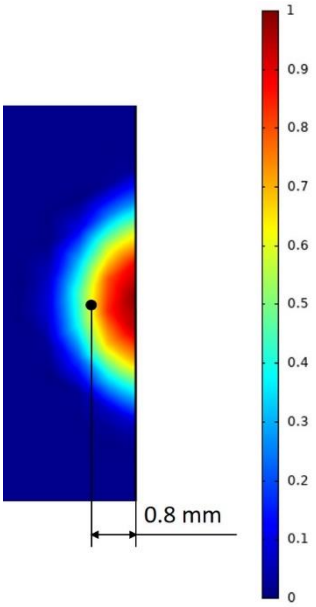

Figure 13. Simulation results of martensite and a prediction of the hardening depth in the AISI 1045 specimen.

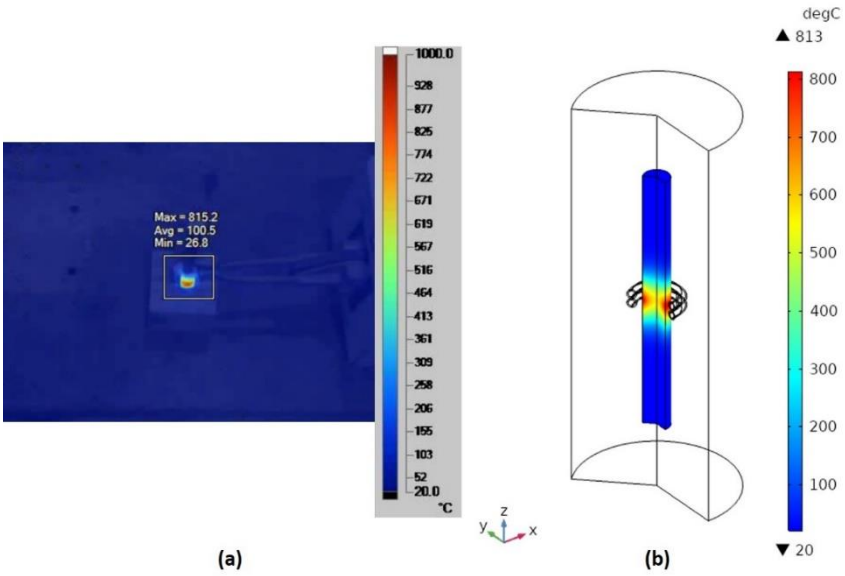

Figure 14. High-frequency induction heating maximum temperatures: from (a) experiments and (b) simulations.

Preprints (www.preprints.org) | NOT PEER-REVIEWED | Posted: 13 October 2020 doi:10.20944/preprints202010.0260.v1

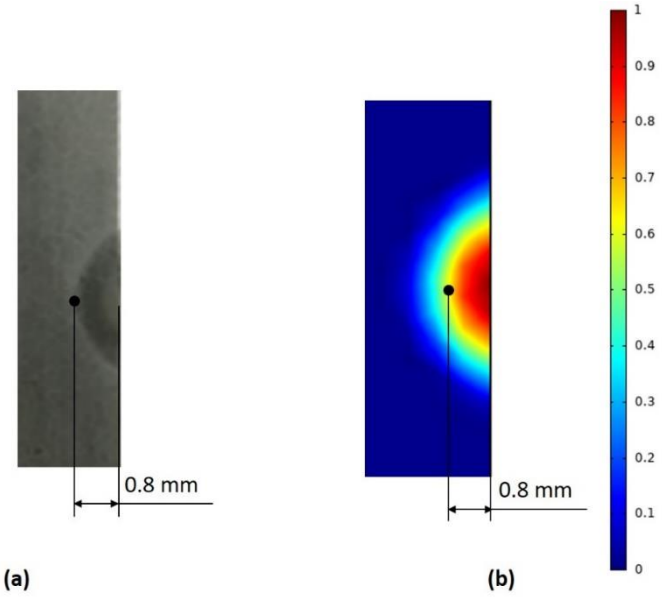

Figure 15. Comparison of hardening depth results: from (a) experiments and (b) simulations.

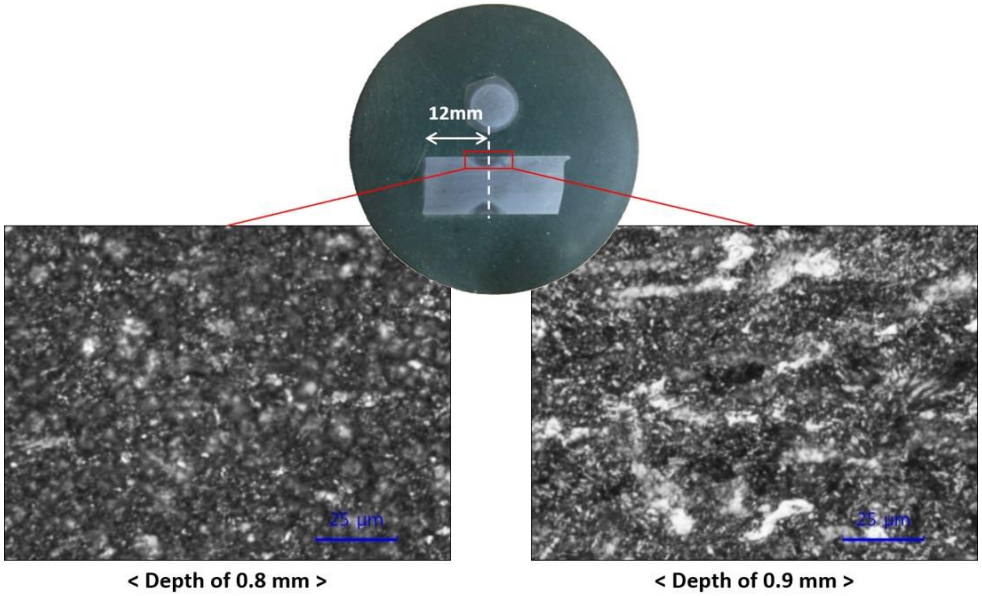

Figure 16. Optical microscopic images of the AISI 1045 specimen and its hardening depth.

5. Comparative verification of experiment and simulation results

High-frequency heat treatment experiments and simulation results of AISI 1045 specimens were compared and verified. The maximum temperature measured during heating was 815.2 ℃, as shown in Fig. 14(a), and the average temperature measured was 798.5 ℃. The simulated maximum heating temperature was 813 ℃, as shown in Fig. 14(b); a 2.2 ℃ difference from the maximum temperature was measured (14.5 ℃ difference from the average temperature). An error of less than 2% occurred in the measurement temperature and simulation temperature results. The hardening depth results of the AISI 1045 specimen were compared. Figure 15(a) shows the results of a high-frequency heat treatment experiment with a curing depth of 0.8 mm (Fig. 4). The predicted hardening depth by simulations was 0.8 mm, as shown in Fig. 15(b); thus, the hardening depth results were consistent. To confirm the metal phase transformation according to the depth of the cured specimen, the specimen was examined with an optical microscope; the image is displayed in Fig. 16. At a hardening

Preprints (www.preprints.org) | NOT PEER-REVIEWED | Posted: 13 October 2020 doi:10.20944/preprints202010.0260.v1

depth of 0.8 mm, the ratio of hardened martensite tissue (black) was high. However, at a hardening depth of 0.9 mm, the proportion of uncured tissue (white) was high. This confirms that the high-frequency heat treatment was correctly simulated to determine the current flowing into the induction coil.

6. Conclusions

This study simulated electromagnetic heat transfer using metal phase transformation models of high-frequency heat treatment of AISI 1045 specimens. Experiments were performed to verify the simulation results, and the resulting hardening depths were compared. Our results and conclusions are summarized below.

1. After converting the high-frequency induction heating system to the RLC circuit, the AC current (708 A) flowing through the induction heating coil was calculated and simulated. The temperature of the induction heating experiment of the AISI 1045 specimens was 798.5 ℃ and the simulated temperature was 813 ℃, with an error rate of 1.8%.
2. To verify the hardening depth obtained by simulations, experiments were conducted, which produced the same 0.8 mm hardening depth.
3. The results of experiments and simulations matched well. Phase transformation simulations were more intuitive and efficient than previous simulations predicting the curing area using only the existing heating and cooling temperatures [7,8]. It is expected that the high-frequency heat treatment and the heating coil shape can be further optimized through electromagnetic-thermal transfer and phase transformation simulations.

Author Contributions: Conceptualization, J.C. and S.L.; methodology, J.C.; software, J.C.; validation, J.C. and S.L.; formal analysis, J.C.; investigation, J.C.; resources, J.C.; data curation, J.C.; writing—original draft preparation, J.C.; writing—review and editing, J.C.; visualization, J.C.; supervision, S.L.; project administration, S.L.; funding acquisition, S.L. All authors have read and agreed to the published version of the manuscript.

Funding: This work was supported by the National Research Foundation of Korea(NRF) grant funded by the Korea government(MSIT) (No. 2020R1F1A106598311) and GNU Graduate Education and Researcher Program for Mechanical and Aerospace Engineers

Conflicts of Interest: The authors declare no conflict of interest.

The English in this document has been checked by at least two professional editors, both native speakers of English. For a certificate, please see: http://www.textcheck.com/certificate/rYHHfY

References

1. Y. Han, E. Yu, H. Zhang, D. Huang, "Numerical analysis on the medium-frequency induction heat treatment of welded pipe", Journal of Applied Thermal Engineering, 51, pp.212-217, 2013. (https://doi.org/10.1016/j.applthermaleng.2012.08.032)
2. H. Li, L. He, K. Gai, R. Jiang, C. Zhang, M. Li, "Numerical simulation and experimental investigation on the induction hardening of a ball screw", Journal of Materials and Design, 87, pp.863-876, 2015. (https://doi.org/10.1016/j.matdes.2015.08.094)
3. I. Y. Lee, S. M. Tak, I. S. Pack and S. S. Lee, "Comparative Study on Numerical Analysis using Co-simulation and Experimental Results for High Frequency Induction Heating on SCM440 Round Bar", Journal of the Society for Aerospace System Engineering, Vol. 11, No. 3, pp.1-7, 2017. (https://doi.org/10.20910/JASE.2017.11.3.1)

Preprints (www.preprints.org) | NOT PEER-REVIEWED | Posted: 13 October 2020 doi:10.20944/preprints202010.0260.v1

4. D. W. Oh, T. H. Kim, K. H. Do, J. M. Park, J. H. Lee, "Design and Sensitivity Analysis of Design Factors for Induction Heating System", Journal of the Korean Society for Heat Treatment, Vol. 26, No. 5, pp.233-240, 2013. (http://dx.doi.org/10.12656/jksht.2013.26.5.233)
5. H. Ji, B. Wang, X. Fu, "Study on the induction heating of the workpiece before gear rolling process", Proceeding of the 20th International ESAFORM Conference on Material Forming, Vol. 1896, No. 120010, pp.1-6, 2017. (https://doi.org/10.1063/1.5008148)
6. S. M. Tak, H. B. Kang, I. S. Baek and S. S. Lee, "Improved workability using preheating in the electromagnetic forming process", Journal of Mechanical Science and Technology, Vol. 33, No. 6, pp.2809-2815, 2019. (https://doi.org/10.1007/s12206-019-0527-3)
7. J. K. Choi, K. S. Park and S. S. Lee, "Predicting the hardening depth of a sprocket by finite element analysis and its experimental validation for an induction hardening process", Journal of Mechanical Science and Technology, Vol. 32, No. 3, pp.1235-1241, 2018. (https://doi.org/10.1007/s12206-018-0227-4)
8. J. K. Choi, K. S. Park and S. S. Lee, "Prediction of High-Frequency Induction Hardening Depth of an AISI 1045 Specimen by Finite Element Analysis and Experiments", International Journal of Precision Engineering and Manufacturing, Vol. 19, No. 12, pp.1821-1827, 2018. (https://doi.org/10.1007/s12541-018-0210-0)
9. D. Tong, J. Gu and G. E. Totten, "Numerical simulation of induction hardening of a cylindrical part based on multi-physics coupling", Modelling and Simulation in Materials Science and Engineering, Vol. 25, No.3, 035009, 2017. (https://doi.org/10.1088/1361-651X/aa5f7c)
10. V. Rudnev, D. loveless, R. Cook, M. Black, "Handbook of Induction Heating", Marcel Dekker, pp.19.
11. KS D 0027, “Methods of Measuring Case Depth for Steel Hardened by Flame or Induction Hardening Process,” Korean Agency for Technology and Standards, 2002.
12. C. Alexander, M. O. Sadiku, "Fundamentals of Electric Circuits", McGraw-Hill, pp.613-673.
13. Kai Gaoa, Xunpeng Qin, Zhou Wang, Hao Chen, Shengxiao Zhu, Yanxiong Liu, Yanli Song, "Numerical and experimental analysis of 3D spot induction hardening of AISI 1045 steel," Journal of Materials Processing Technology, Vol. 214, pp. 2425-2433, 2014. (https://doi.org/10.1016/j.jmatprotec.2014.05.010)
14. J. B. Leblond, J, Devaux, " A New Kinetic Model for Anisothermal Metallurgical Transformations in Steels Including Effect of Austenite Grain Size," Acta metall., Vol. 32, No. 1, pp. 136-146, 1984. (https://doi.org/10.1016/0001-6160(84)90211-6)
15. D. Koistinen and R. Marburger, “A general equation prescribing the extent of the austenite-martensite transformation in pure iron-carbon alloys and plain carbon steels,” Acta Metall., vol. 7, p. 5960, 1959. (https://doi.org/10.1016/0001-6160(59)90170-1)
16. W. Edelbauer, D. Zhang, R. Kopun, B. Stauder, "Numerical and experimental investigation of the spray quenching process with an euler-eulerian multi-fluid model," Applied Thermal Engineering, Vol. 100, pp. 1259-1273, 2016. (https://doi.org/10.1016/j.applthermaleng.2016.02.131)